Journal of Molecular Structure 1294 (2023) 136430

Contents lists available at ScienceDirect

Journal of Molecular Structure

journal homepage: www.elsevier.com/locate/molstr

Computational and spectroscopic analysis of the Quercetin encapsulation in $(2HP\text{-}\beta\text{-}CD)_2$ and $(2,6Me\text{-}\beta\text{-}CD)_2$ complexes

Georgios Leonis [a], Vasiliki Vakali [a], Nikoletta Zoupanou [a], Nikitas Georgiou [a], Dimitrios A. Diamantis [b], Andreas G. Tzakos [b,c], Thomas Mavromoustakos [a], Demeter Tzeli [d,e,*]

[a] Department of Chemistry, Organic Chemistry Laboratory, National and Kapodistrian University of Athens, PanepistimiopollisZografou 11571 Athens, Greece
[b] Department of Chemistry, Section of Organic Chemistry and Biochemistry, University of Ioannina, 45110 Ioannina, Greece
[c] University Research Center of Ioannina (URCI), Institute of Materials Science and Computing, 45110 Ioannina, Greece
[d] Department of Chemistry, Physical Chemistry Laboratory, National and Kapodistrian University of Athens, PanepistimiopolisZografou, 11571 Athens, Greece
[e] Theoretical and Physical Chemistry Institute, National Hellenic Research Foundation, 11635 Athens, Greece

ARTICLE INFO

Keywords:
Quercetin
2-hydroxyl-propyl-β-cyclodextrin
2,6-methylated-β-cyclodextrin
Molecular interactions
NMR spectroscopy
Fluorescence spectroscopy
DFT calculations
Cyclodextrin
Encapsulation

ABSTRACT

Quercetin protects against many diseases due to its radical scavenging and anti-inflammatory properties. However, due to its poor bioavailability numerous types of nanocarriers have been evolved to increase quercetin solubility and to design tissue-specific delivery systems. Here, we study the entrapment of quercetin(QUE) in two dimeric assemblies formed by 2HP-β-CD and 2,6Me-β-CD, employing DFT calculations, NMR and fluorescent spectroscopy. Via NMR and fluorescent spectroscopy, it was revealed that the QUE:CDs stoichiometry for optimal complex formation follows a 1:2 pattern. DFT indicated that although both dimeric assemblies of 2HP-β-CD and 2,6Me-β-CD, as well as their encapsulation quercetin complexes are stable, the former dimer and the QUE@2HP-$\beta\text{-}CD_2$ complex demonstrate the highest level of stability. The absorption spectrum of QUE in CD and CD_2 was calculated. Encapsulation influences it, resulting in red and blue shifts, and in differences in the intensities. Only, the dimeric assemblies affect the electron density of QUE resulting in major peaks at about 250 nm, which are charge transfer (CT) or partially CT excitations. Finally, for the encapsulated QUE in CDs, the calculated $T_1 \rightarrow S_0$ vertical de-excitation is about 570 nm in the single CDs and about 800 nm in the dimeric complexes, making these complexes potential candidates for PDT.

1. Introduction

Cancer is a growing health problem, currently being the second most common cause of death worldwide, after heart attacks [1]. The formation of a malignant neoplasmis guided by uncontrollable growth of abnormal cells, which divide and spread to organs or tissues of the body. The main reason that hinders a complete therapy of cancer is that the various cancerous tumors progress heterogeneously and behave differently at the molecular, morphological and genetic level [2]. Also, common chemotherapeutics are often unable to achieve the expected therapeutic outcomes, as a consequence of their limited solubility, rapid metabolism, and a lack of targeting efficiency [3].

Recently, natural products have gained significant attention in the rational anti-cancer drug development, due to their antitumor effectiveness and abundance of potential candidates. It has been observed that natural drugs are generally safe, and present diminished side effects compared with the synthetic compounds, thus resulting in enhanced immunity and optimized chemotherapy sensitivity. Flavonoids are natural nutritional compounds, which exert anti-oxidant, anti-fungal, anti-inflammatory, and anti-bacterial actions [4]. Flavonoids and their metabolites regulate carcinogenesis by multiple signal transduction pathways [5]. Various subfamilies of flavonoids include flavanones, flavones, isoflavones, and flavonols. Quercetin (QUE) (3,3′,4′,5,7-pentahydroxy flavone, Scheme 1) is a flavone-type flavonoid, which is found in vegetables, tea, fruits, and wine in its glycoside form. QUE is metabolized in the human body to sugar conjugates, including quercitrin, isoquercitrin, and rutin. Metabolism of QUE occurs in the intestine and liver.

After multiple research efforts, QUE has been established as both anti-oxidant and pro-oxidant agent, depending on the redox state of cells and QUE concentration [6]. It is known that QUE suppresses the proliferation of multiple cell lines related to human breast cancer [7].

* Corresponding author.
E-mail address: tzeli@chem.uoa.gr (D. Tzeli).

https://doi.org/10.1016/j.molstruc.2023.136430
Received 1 April 2023; Received in revised form 11 August 2023; Accepted 14 August 2023
Available online 15 August 2023

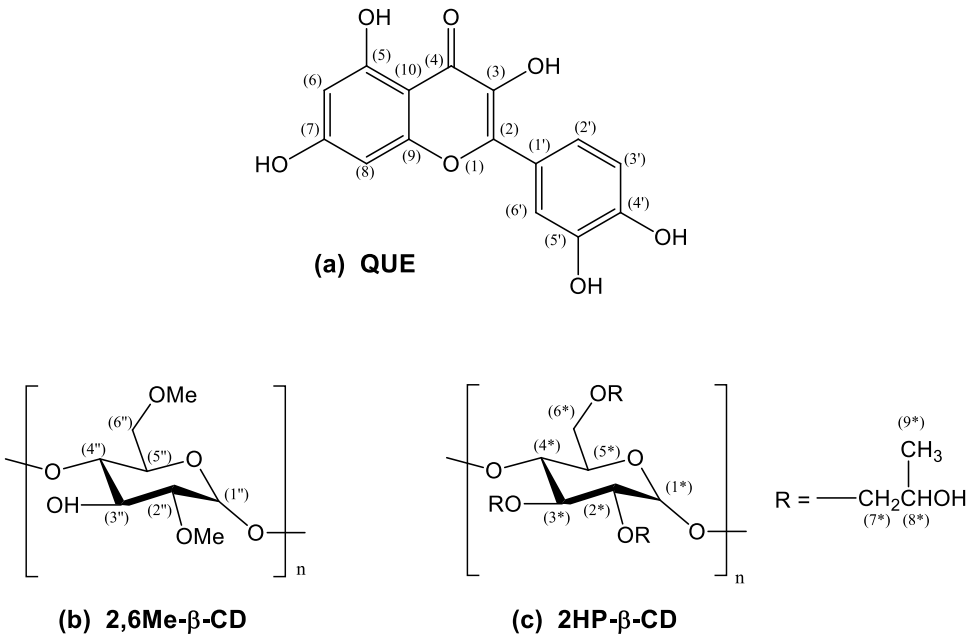

Scheme 1. Chemical structures of (a) quercetin (QUE); (b) 2,6-methylated cyclodextrin (2,6Me-β-CD) and (c) 2-hydroxyl-propyl-β-cyclodextrin (2HP-β-CD), $n = 7$.

Attributable to its pro-oxidant ability, QUE assists the obstruction of tumor growth. In addition, QUE urges the induction of apoptosis and leads to cell cycle arrest [8]. Furthermore, QUE shows anti-cancer properties by growth inhibition and pro-apoptosis effects [9]. A recent study revealed that QUE restricts the Janus kinase–signal transducer and activator of transcription (JAK-STAT) and NF-kB activation, while it also prevents inducible nitric oxide synthase (iNOS) expression and NO production [10]. Importantly, QUE has been associated with beneficial effects in cancer treatment [9,11].

Despite the potential beneficial actions of QUE, this compound displays chemical instability, poor water solubility, and low bioavailability. These features result in reduced pharmaceutical efficacy for QUE. To overcome problems of this kind, proper delivery systems have been developed, aiming at the effective encapsulation of functional small molecules to protect them against degradation and to effectively carry them by also increasing their bioavailability. For this purpose, several molecular transporters have been used as efficient drug carriers, including microparticles, microemulsions, nanoemulsions, and nanoparticles [12].

For the past few years, cyclodextrins (CDs) are recognized as effective excipients to facilitate drug delivery for various drug formulations. CDs are a group of cyclic oligosaccharides composed of glucopyranose units, linked by 1,4-glycosidic bonds. According to the number of glucose units, one can distinguish α-, β- and γ-CD, which contain 6, 7, and 8 units, respectively. Apart from these widely known CDs, many derivatives have been synthesized, such as 2-hydroxy-propyl-β-cyclodextrin (2HP-β-CD), and 2,6-methylated cyclodextrin (2,6Me-β-CD) (Scheme 1). CD structures have a conical-type shape and comprise a hydrophilic exterior, which surrounds a lipophilic inner cavity [13]. Such a structure enables the entrapment of hydrophobic molecules and favors the formation of stable host–guest complexes. Consequently, the water solubility and in turn, the bioavailability of the entrapped molecules may be increased for broad pharmacological applications [14–16].

Currently, CDs are widely used for improvements in solubility, stability, loading and release capacity of hydrophobic compounds (e.g., natural products as potential drug candidates),while in the same time retaining their bioactivity and abolishing potential toxicity [17–19]. Numerous cases of stable natural product–CD complexes have been reported, such as for silibinin, QUE, isoquercitrin, taxifolin, losartan, and cholesterol [20–22]. The outcomes verify the favorable complexation between natural products and different forms of CD; in particular, for QUE complexed with β-CD and 2HP-β-CD, previous molecular docking and natural bond orbital (NBO) calculations suggested a significant degree of stability for the corresponding inclusion complexes in 1:1 stoichiometry [23]. Additionally, in most cases, it was observed that complexation was accompanied by a significant optimization of the pharmacological properties. Also, various research studies revealed that nanocarriers containing cyclodextrin favor the encapsulation of anti-cancer agents, including flavonoids, for effective cancer therapy [12,24].

Recently, we studied the interaction of QUE with 2HP-β-CD and 2,6Me-β-CD via NMR spectroscopy, DFT calculations, molecular dynamics (MD) simulations, and fluorescent spectroscopy [25]. Energetic, structural, and dynamic properties of complex formation were explored and combined into a comprehensive scheme that showed adequate binding of QUE to both CD formulations (i.e., 2HP-β-CD and 2, 6Me-β-CD). Furthermore, phase solubility studies in a mixture of QUE with 2HP-β-CD or 2,6Me-β-CD [20] show a positive deviation from the linearity, observed mainly in 2HP-β-CD at pH 6.8, which could be attributed to the further formation of a 1:2 (QUE/CD) complex. Thus, in the present work, we attempt to deepen our understanding on the binding modes of QUE with the aforementioned CDs by investigating the requisite QUE:CDs stoichiometry that gives rise to favorable complexation. Specifically, we study the entrapment of QUE in two capsules, i.e., dimeric assemblies, formed by 2HP-β-CD and 2,6Me-β-CD, employing NMR and fluorescent spectroscopy, and DFT calculations. In the CD cage, QUE is isolated from the solvent through mechanical barriers, so that its lipophilicity may be relieved and thus it can effectively be carried in water solutions. In fact, the CD capsule functions as the solvent, surrounding the solute. Furthermore, the absorption spectra of free and encapsulated QUE in cavitands and in their dimeric assemblies is calculated via TD-FFT methodology. Intriguingly, it was revealed that the QUE:CDs stoichiometry for optimal complex formation follows a 1:2 pattern, where one QUE molecule is associated with two different CD molecules (namely, 2HP-β-CD and 2,6Me-β-CD).

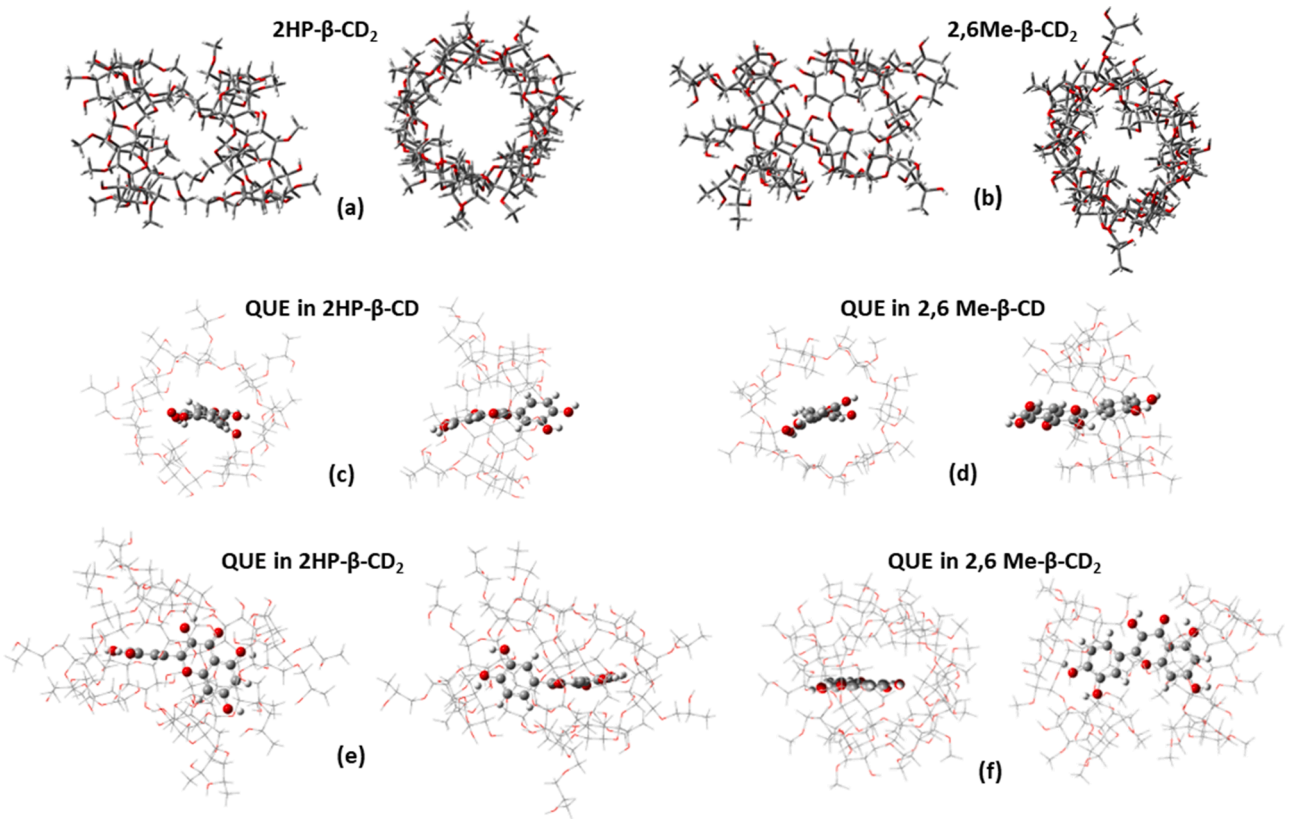

Fig. 1. Calculated minimum energy structures: (a) 2HP-β-CD_2 dimeric assembly, (b) 2,6Me-β-CD_2 dimeric assembly, (c) QUE@2HP-β-CD, (d) QUE@2,6Me-β-CD, (e) QUE@2HP-β-CD_2, and (f) QUE@2,6Me-β-CD_2.

2. Material and methods

2.1. DFT calculations

The interactions between the two cyclodextrins and the QUE were calculated using the semi-empirical PM6 methodology [26], the ONIOM (B3LYP/6-31G(d,p):PM6) and ONIOM(B3LYP/6-311+G(d,p):PM6) methods [27–29] in water solvent. In the ONIOM methodology, the QUE@CD_2 systems are defined as two regions (layers). The high layer is the QUE molecule calculated at the B3LYP/6-31G(d,p) or B3LYP/6-311+G(d,p) level of theory and the low layer is the CD_2 dimer calculated at the PM6 level of theory. The calculated encapsulated systems have 410 and 466 atoms, making the use of the DFT methodology for the whole system very time consuming. The use of ONIOM methodology is regarding as appropriate giving good results in agreement with the full DFT calculations [27,30–32] and the use of the B3LYP functional is sufficient for the present calculations [25,30,33].

At first, the dimer CDs, i.e., 2HP-β-CD_2 and 2,6Me-β-CD_2, and the encapsulation complexes, i.e., QUE@2HP-β-CD_2 and QUE@2,6Me-β-CD_2 were optimized using PM6 methodology. Note that as initial guess geometry for each CD cavitand was used its energy optimized B3LYP/6-31G(d,p) geometry of 25. Conformational analysis for the dimers i.e., 2HP-β-CD_2 and 2,6Me-β-CD_2, and their encapsulation complexes was carried out to find the lowest in energy minima. Then for both QUE@2HP-β-CD_2 and QUE@2,6Me-β-CD_2ONIOM(B3LYP/6-31G(d,p):PM6) calculations were carried out for the lowest in energy singlet state, S_0, and the lowest in energy triplet state.

Via the TD-DFT methodology, the absorption spectra of the encapsulated QUE were calculated in a single CD and in dimeric assemblies CD_2. Note, that ONIOM methodology assists to separate the spectra of the QUE from the spectra of CD dimers [30]. Thus, for these optimized geometries, both absorption spectra have been calculated at ONIOM (B3LYP/6-311+G(d,p):PM6) for the 2HP-β-CD_2 and QUE@2,6Me-β-CD_2 complexes and at B3LYP/6-311+G(d,p) for the QUE at its encapsulated geometry employing a dielectric constant and PCM model [34]. It is known that the dielectric constants in CD cavities is estimated at about 48–55 in CDs [35], while in aqueous alkaline solutions where QUE is solved, is estimated at 71 [36]. Calculations were carried out employing dielectric constants of 48, 71 and 78 and the absorption peaks differences are very small, i.e., they range from 0.1 to 1.4 nm. Finally, the NMR spectrum of the QUE molecule free and encapsulated in one CD and in dimeric assemblies were computed. All calculations were performed in aqueous solution employing the polarizable continuum model (PCM) [36]. All calculations and the visualization of the results was carried out via Gaussian 16 [37].

2.2. NMR spectroscopy

QUE (MW: 302.24 g/mol), 2,6Me-β-CD (MW: 1310 g/mol) and 2HP-β-CD (MW: 1460 g/mol) were purchased from Sigma-Aldrich (St. Louis, MO, USA), Fluka Chemika (Mexico City, Mexico US & Canada) and Ashland (Covington, KY, USA), respectively. The NMR experiments were performed, using the core facility AVANCE NEO 500 MHz spectrometer - Bruker Biospin. For the preparation of samples was needed 15 mg of QUE, 2,6Me-β-CD, 2HP-β-CD as control samples, and a quantity of ca 15 mg mixture and complex of QUE:2HP-β-CD and QUE:2,6Me-β-CD using the stoichiometry ratio 2:1. All samples were diluted in 750 μL of D_2O and DMSO-d6 and prepared for NMR experiments. The structural elucidation was achieved by analysis of standard 1D experiment (^1H) at 25 °C (room temperature) and 40 °C. Parameters of the 1D experiments were extracted from the regular library installed in the NMR spectrometer. Spectra were received, analyzed and processed using standard Bruker NMR software (Topspin 3.5) and MestreNovasoftware. The experiments were performed three times and the RMSD values for the

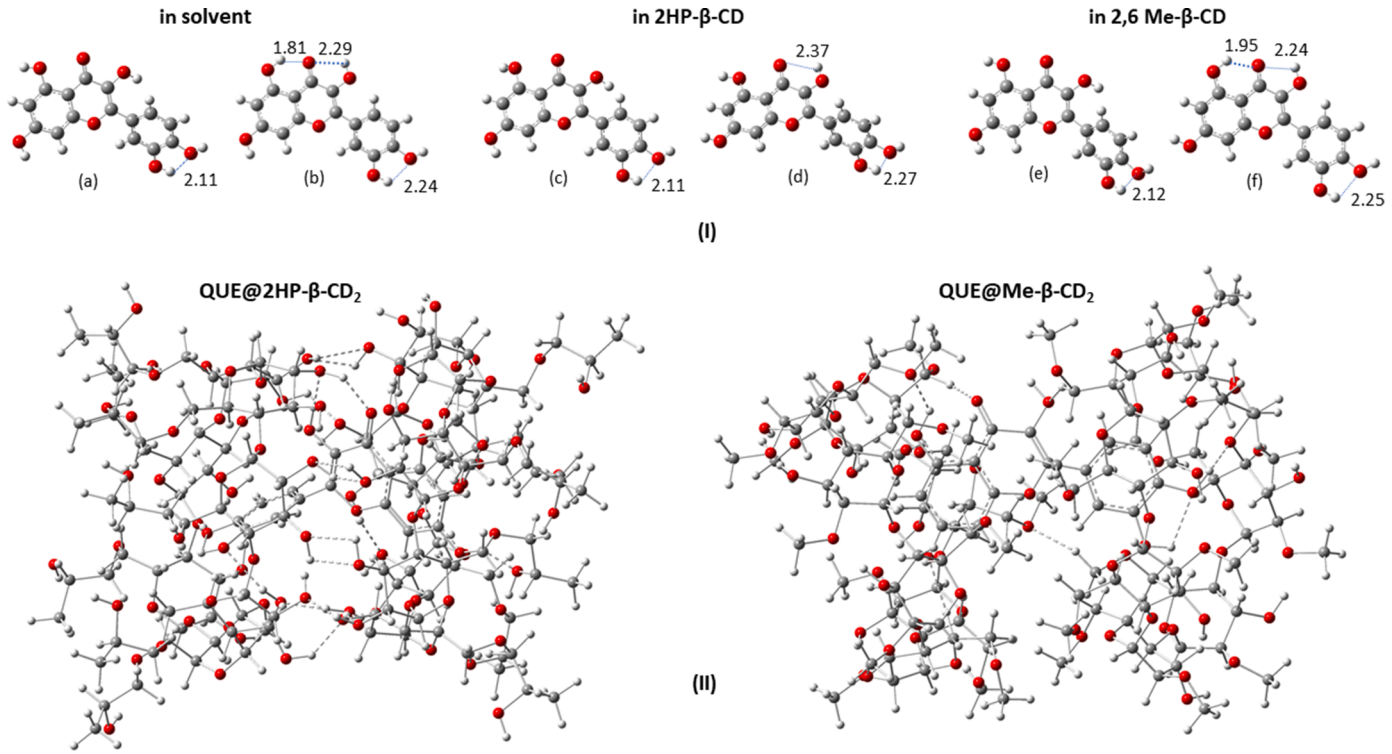

Fig. 2. Formation of hydrogen bonds (dashed lines) in: (I) Conformations of (a) QUE local minima, (b) QUE global minima, (c) QUE in the complex of 2HP-β-CD, (d) QUE in 2HP-β-CD dimeric assembly (e) QUE in 2,6Me-β-CD (f) QUE in 2,6Me-β-CD dimeric assembly calculated at the B3LYP/6-311+G(d,p) level of theory; (II) Minimum structures of (g) QUE@2HP-β-CD_2 and (h) QUE@2,6Me-β-CD_2.

average differed by ±0.001. The degree of substation of the 2HP-β-CD host molecule varied by 2 up to 9 groups [38].

2.3. Fluorescence spectroscopy

Fluorescence spectroscopy experiments were conducted to determine the stoichiometry of QUE complexes with 2HP-β-CD and 2,6Me-β-CD, respectively. The experiments were performed in an Edinburg FS5 spectrofluorometer (Edinburgh Instruments Ltd., Livingston, UK). The excitation and emission slits were set at 5 nm and the emission spectra were recorded using a quartz (1 cm cuvette), at room temperature. A stock solution of QUE (3 mM) was prepared in DMSO followed by the preparation of the CD stock solutions (3 mM) in dd water. Then, into a small vial containing 2924 μL of the solvent 2 μL of QUE were added followed by the addition of 74 μL dd H_2O. The vial was well mixed, and the fluorescence spectrum was recorded. This experiment was repeated one more time, however 38 μL of the dd H_2O was replaced by 38 μL of the cyclodextrin stock solution and the fluorescence spectrum was further recorded. The maxima values of the λ_{em} spectra were noticed and the ΔF value was extracted. The same procedure was repeated for each one different molecular fraction of QUE. The stoichiometry of the formed complexes was determined using Job's plot method by plotting the alternation of the fluorescent signal at 550 nm against the molar fraction.

3. Results and discussion

3.1. DFT calculations

3.1.1. Geometry and energetics

The calculated geometries of the complexes are shown in Figs. 1 and 2 and in Figs. 1S-3S of SI. The hydrogen bonds are formed between the two CDs and between CDs with QUE. Specifically, ten hydrogen bonds are formed that range from 1.8 to 2.5 Å in the case of 2HP-β-CD dimeric assembly, and two hydrogen bonds are formed in the case of 2,6Me-β-CD dimeric assembly with bond distances up to 2.8 Å and additional two bonds up to 3 Å, see Fig. 2 and 1S–3S of SI. Thus, we conclude that the 2HP-β-CD_2 dimeric assembly is more stable than 2,6Me-β-CD_2. In the case of QUE@2HP-β-CD_2 and QUE@2,6Me-β-CD_2, six hydrogen bonds are formed between 2HP-β-CD dimeric assembly complex with QUE and five hydrogen bonds in the case of 2,6Me-β-CD_2 dimeric assembly complex with QUE with bond distances less than 2.8 Å, see Figs. 2 and S1–S3 of SI. Note that the QUE molecule in 2HP-β-CD_2 is better encapsulated than in 2,6Me-β-CD_2, c.f. Fig. 1e and f. In the second assembly, QUE prefers to form H-bonds with the 2,6Me-β-CD cavitands and further stabilizes the dimeric assembly, see Figs. 1, 2 and S2–S3 if SI. This occurs because the 2HP-β-CD has terminal -OH groups that form bonds with the second 2HP-β-CD cavitand, resulting in a stabilization of the 2HP-β-CD_2 dimeric assembly. On the contrary, the 2,6Me-β-CD cavitand has -OMe terminal groups and thus the dimeric assembly is stabilized with the weak van der Waals bonds between the oxygen of -OMe and the hydrogen atoms of the -OMe group. Thus, the role of QUE is important in the stabilization of the QUE@2,6Me-β-CD_2 because the QUE's -OH groups form H-bonds with the O of the CD's -OMe group.

On the contrary, regarding the encapsulation of QUE in a single CD, the encapsulation in both CDs is similar, compare Fig. 1c and d, and QUE binds favorably to both 2,6Me-β-CD and 2HP-β-CD [25]. Regarding the encapsulation of QUE, in both single CDs (2HP-β-CD or 2,6Me-β-CD) and in 2HP-β-CD_2 dimeric assembly, is stabilized in a local minimum structure (Fig. 2) so as to form additional bonding the CDs. On the contrary, in 2,6Me-β-CD_2 dimeric assembly, QUE adopts the conformation of its global minimum, resulting in the formation of less additional bonging with the dimeric assembly than in 2HP-β-CD_2 and the encapsulation binding is less strong, (see Fig. 1). Note that 2HP-β-CD is generally more reactive towards substitution reactions compared to their secondary side due to the primary hydroxyl groups being more exposed and accessible for reactions [39].

Energetically, the encapsulated QUE are higher in energy than the

Table 1
Relative energies of the QUE conformations, RE (kcal/mol), Binding Energies of the QUE with CD cavitands, BE (kcal/mol).

	RE[a]	BE[b]
QUE (global minimum)	0.00	
QUE (local minimum)	3.98	
QUE@2HP-β-CD	7.47	−32.95[c] (−31.73 ± 3.21)[c,d]
QUE@2,6Me-β-CD	4.38	−24.21[c] (−26.77 ± 2.37)[c,d]
QUE@2HP-β-CD_2	18.54	−49.52
QUE@2,6Me-β-CD_2	5.84	−27.70

[a] B3LYP/6-311+G(d,p).
[b] b3LYP/6-31G(d,p).
[c] Ref [25].
[d] MM/GBSA.

Table 2
B3LYP/6-311+G(d,p) values in ppm of QUE alone, QUE with 2,6Me-β-CD (stoichiometry ratio 1:2) and QUE with 2,6Me-β-CD in D_2O at 25 °C (stoichiometry ratio 1:2) in comparison with present experimental data.

		H6′	H2′	H3′	H8	H6a	H6b
QUE alone	**DFT**	8.03	8.40	7.24	6.66	6.71	6.71
	Expt	7.703	7.600	7.028	6.693	5.865	5.892
Complex (QUE & 2,6Me -β-CD): QUE@2,6Me-β-CD_2	**DFT**	8.32	9.04	7.28	6.93	6.46	6.46
	Expt	8.403	7.608	7.544	6.921	6.634	6.291
Complex (QUE &2HP-β-CD): QUE &2HP-β-CD_2	**DFT**	7.42	7.38	7.42	6.91	6.46	6.46
	Expt	8.397	7.575	7.431	6.913	6.565	6.218

Table 3
Absorption $S_0 \rightarrow S_x$ and $S_0 \rightarrow T_1$ excitations, λ (nm), energy differences ΔE (eV), f-values, and the corresponding main excitations of free QUE (global minimum) and QUE (local minima) and encapsulated QUE in 2HP-β-CD, in 2,6Me-β-CD and in their dimeric assembly calculated at the B3LYP/6-311+G(d,p) and ONIOM (B3LYP/6-311+G(d,p):PM6) level of theory.

State	λ	ΔE	f	main Conf	λ	ΔE	f	main Conf
	QUE (global) in aqueous solution				**QUE (local) in aqueous solution**			
T_1	513.9	2.41		**H→L**	489.0	2.54		**H→L**
S_1	372.5	3.33	0.511	**H→L**	349.3	3.55	0.438	**H→L**
S_a	269.0	4.61	0.189	**H →L + 1**	268.7	4.61	0.158	**H →L + 1**
S_b	212.1	5.84	0.112	**H-2→L + 2**	210.5	5.89	0.333	**H-3→L + 2**
S_c	202.2	6.16	0.330	**H-6 →L**	200.0	6.20	0.324	**H-3→L + 3**
	QUE in 2HP-β-CD				**QUE in 2,6Me-β-CD**			
T_1	487.4	2.54		**H→L**	491.4	2.52		**H→L**
S_1	350.3	3.54	0.428	**H→L**	350.3	3.54	0.454	**H→L**
S_a	263.9	4.70	0.173	**H→L + 2**	268.7	4.61	0.179	**H →L + 1**
S_b	204.3	6.07	0.241	**H-3→L + 3**	210.0	5.90	0.279	**H-5 →L + 2**
S_c	201.9	6.14	0.262	**H-3→L + 3**	200.0	6.20	0.406	**H-3 →L + 3**
	QUE in 2HP-β-CD_2				**QUE in 2,6Me-β-CD_2**			
T_1	453.8	2.73		**H→L**	533.8	2.32		**H→L**
S_1	331.6	3.74	0.228	**H→L**	379.4	3.27	0.554	**H→L**
S_a	250.5	4.95	0.454	**H →L + 2**	269.0	4.61	0.182	**H →L + 1**
S_b	203.3	6.10	0.186	**H-2 →L + 6**	210.1	5.91	0.274	**H-2 →L + 2**
S_c	200.2	6.19	0.287	**H-4 →L + 1**	201.6	6.2	0.4	**H-2 →L + 3**

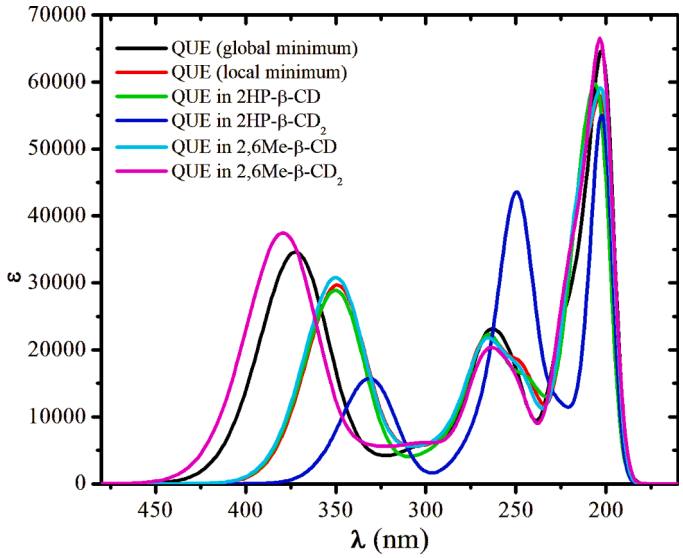

Fig. 3. Absorption Spectra of QUE free in aqueous solution and encapsulated in 2HP-β-CD, 2HP-β-CD_2, 2,6Me-β-CD, and 2,6Me-β-CD_2 assemblies at the B3LYP/6-311+G(d,p) method.

global minimum; their relative energies with respect to the global minimum ranges from 4.4 to 18.5 kcal/mol, see Table 1. The highest in energy conformation is observed in QUE@2HP-β-CD_2 dimeric assembly, since the phenyl group is rotated with respect to the benzopyran, see Fig. 1, so as to be encapsulated efficiently in the 2HP-β-CD_2. Regarding the binding energy of QUE with CD or CD_2, we found that QUE binds favorably in both single CDs with a BE of −33.0 kcal/mol and −24.2 kcal/mol for 2HP-β-CD and 2,6Me-β-CD, respectively [25]. However, in the dimeric assembly, the BE of QUE is almost double in 2HP-β-CD_2, i.e., −49.5 kcal/mol, while in 2,6Me-β-CD_2 is −27.7 kcal/mol, i.e., a similar BE with that when it is encapsulated in a single 2,6Me-β-CD, see Table 1. This shows that the encapsulation is not so favorable as in the case of 2HP-β-CD_2.

3.1.2. NMR spectra

The ^{1}H NMR chemical shifts calculated via the B3LYP/6-311+G(d,p) method and the corresponding experimental chemical shifts are in agreement, see Table 2. With the exception of chemical shift of the H6' for the QUE@2HP-β-CD_2 and of the H2' of the QUE@2,6Me-β-CD_2, in all other cases the differences between experimental and theoretical values are small and the differences range from 0 to 0.8 ppm. The experimental NMR spectra and chemical shifts are given in details below in Section 3.2.

3.1.3. Absorption spectra and molecular orbitals

The λ values, energy differences and oscillator strength values of the main peaks of the vis-UV absorption spectra of the QUE in aqueous solution and of the encapsulated QUE in a single CD and in CDs dimeric assembly are given in Table 3, while their absorption spectra are plotted in Fig. 3. The first main peak of the QUE in solution is calculated at 372.5 nm, in very good agreement with the experimental values that range from 365 to 387 nm [40–42], with respect to different pH values (6.03 to 7.88) [41]. This peak is blue shifted about 27 nm in the local minimum, see Table 3. Note that the encapsulated QUE in a single 2HP-β-CD or in a single 2,6Me-β-CD that corresponds to the local minimum, also presents the same value for the absorption peak, $S_0 \rightarrow S_1$. For the encapsulation in the dimeric assemblies, in the 2,6Me-β-CD_2, the lowest in energy encapsulated complex includes the global minimum of QUE and as a result, the main peaks and the absorption spectra of free and encapsulated QUE are very similar, see Fig. 3. On the contrary, in the 2HP-β-CD_2 cage, the encapsulated QUE is reformed, see above and

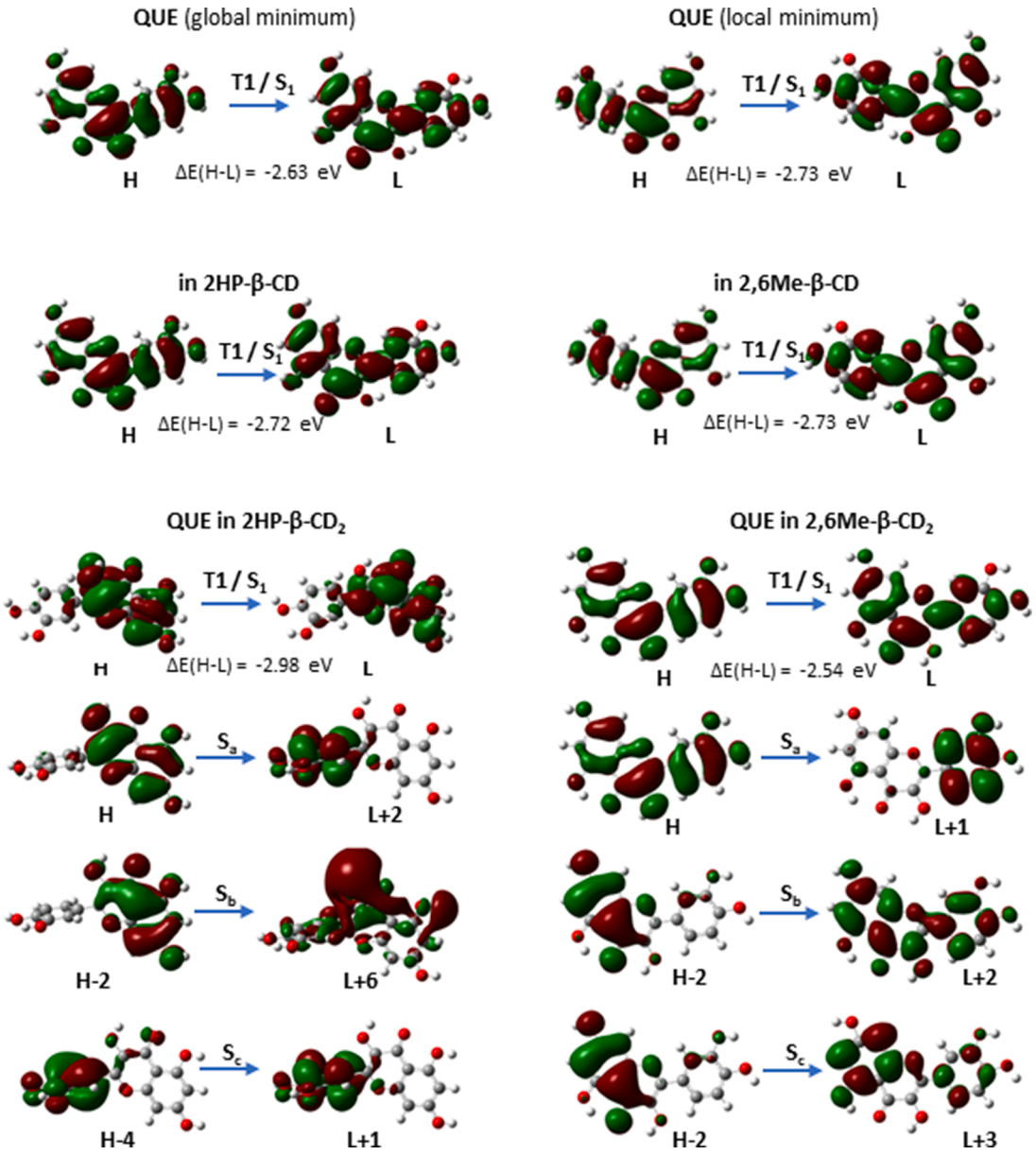

Fig. 4. Frontier Molecular Orbitals of free QUE, encapsulated QUE in a single CD, and encapsulated QUE in dimeric assemblies.

thus the first and the second peaks are blue shifted at 332 and 251 nm, while their intensity has been inversed with respect to remaining five structures, i.e., QUE in aqueous solvent and encapsulated QUE see Fig. 3. It should be noted that experimentally, the second absorption peak is found at 255 nm [42], in good agreement with our data. Finally, similar trends are found for the energetically shifts of the $S_0 \rightarrow T_1$excitation for the six calculated species. The corresponding energy difference ranges from 2.32 to 2.73 eV, i.e., 453.8 nm (QUE in 2HP-β-CD_2) to 533.8 nm (QUE in 2,6Me-β-CD_2).

The molecular orbitals (MO) that are involved in the main absorption peaks are given in Table 3 and they are plotted in Figs. 4 and S4 of SI. It should be noted that the MO of the encapsulated QUE in the single CDs are similar to the local minimum of QUE, see Fig. 2. It is found that in the highest occupied molecular orbital (H) and in the lowest unoccupied molecular orbital (L), the electron density is localized in the whole QUE molecule, see Figs. 4 and S1 of SI, for all cases except QUE in 2HP-β-CD_2 dimeric assembly, where the electron density of both H and L MO is localized in the benzo group, due to the most intent bond interaction of the QUE's -OH group with the cage.

Furthermore, it is of interest that most of the remaining intense excitations S_a, S_b, and S_c correspond to partially charge transfer (CT) excitations or to a full CT one with large oscillator strengths. Specifically, the $S_0 \rightarrow S_a$ excitation corresponds to a partially CT state from the whole QUE molecule to its phenyl group in the cases of the QUE in aqueous solution, of the encapsulated QUE in the single CDs and in dimeric 2,6Me-β-CD_2 assembly. On the contrary, for the QUE in the dimeric 2HP-β-CD_2 assembly, the $S_0 \rightarrow S_a$ excitation is CT excitation from benzopyran to phenyl group, see Fig. 4. It is observed at 251 nm with a significant oscillator strength value of 0.454. Furthermore, the $S_0 \rightarrow S_b$ excitation corresponds to an electron density transfer from the benzopyran to the whole QUE in the cases of QUE in 2,6Me-β-CD_2 and QUE in 2HP-β-CD_2. On the contrary, in the corresponding $S_0 \rightarrow S_c$ excitation the electron density is mainly located at the phenyl group of QUE in the QUE@2HP-β-CD_2, while, it is located mainly at benzopyran of QUE in the QUE@2,6Me-β-CD_2. Finally, the $S_0 \rightarrow S_b$ and the $S_0 \rightarrow S_c$ excitations in free QUE and in single CDs, the electron density is mainly delocalized in the whole molecules with a very small CT character, see Fig. 4.

Finally, the triplet states of the QUE molecule encapsulated in single

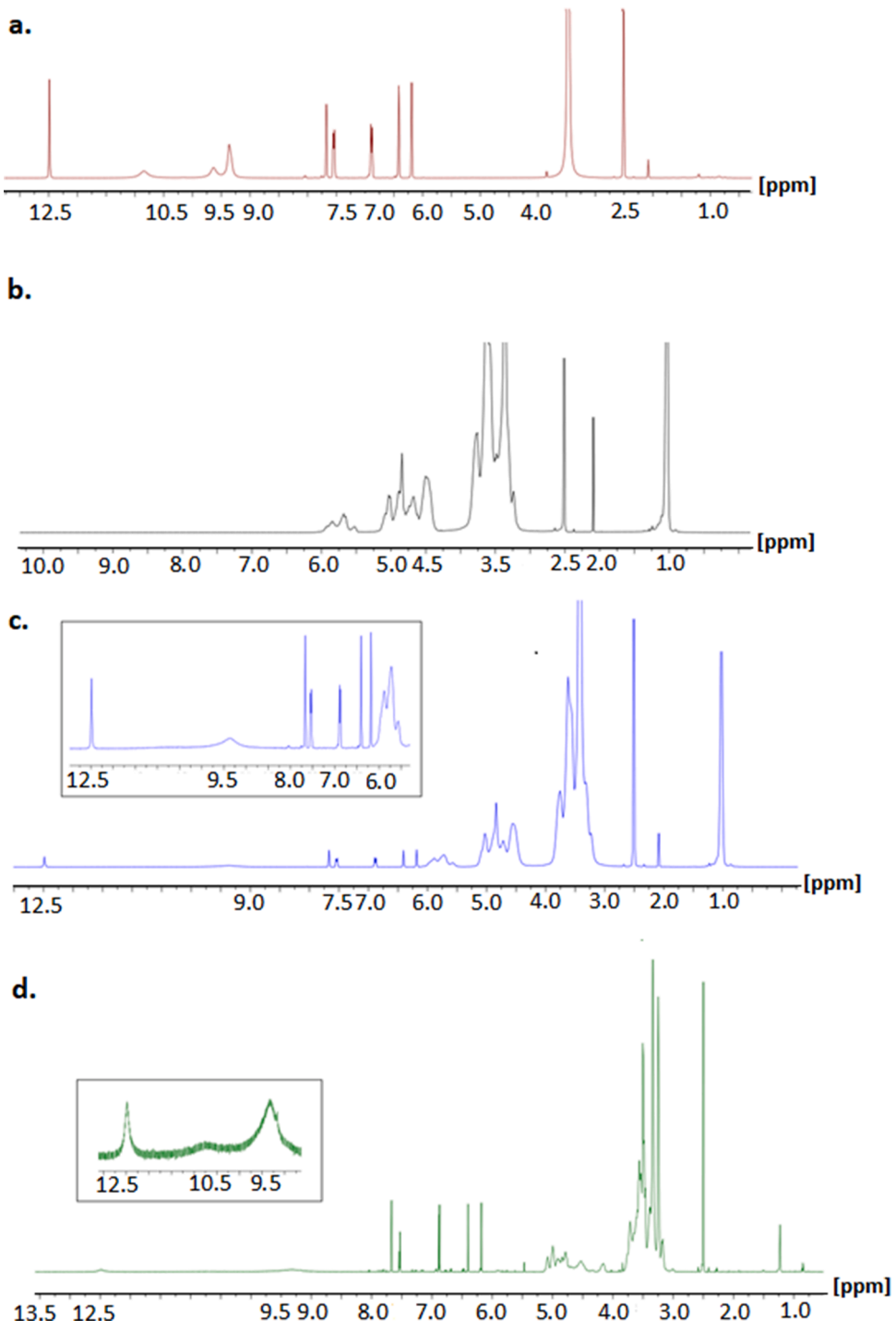

Fig. 5. Spectra of (a) QUE, (b) 2HP-β-CD, (c) mixing of (a) and (b) with a stoichiometry ratio 1:2 and (d) dissolution of the complex of QUE with 2HP-β-CD (ratio 1:2) in DMSO-d6 at 25 °C using a 400 MHz spectrometer.

CDs and dimeric assemblies were calculated, since they are involved in PDT. The photosensitizers that are activated by absorption of visible light to initially form the excited singlet followed by transition to the long-lived excited triplet state. This triplet state can undergo photochemical reactions in the presence of oxygen to form reactive oxygen species (including singlet oxygen) that can destroy cancer cells and pathogenic microbes. For the encapsulated QUE in CDs, the $T_1 \rightarrow S_0$ vertical de-excitation were calculated at 541 nm and 576 nm for the single 2HP-β-CD and 2,6Me-β-CD, respectively, while in the dimeric assemblies, the vertical de-excitation is found at 824 and 794 nm respectively, making them a good candidate for PDT [43,44].

3.2. NMR spectroscopy

Fig. 5 shows ^{1}H NMR spectra of QUE and 2HP-β-CD alone and their mixture using the stoichiometry ratio QUE/2HP-β-CD 2:1 in DMSO-d6 and their complex (stoichiometry ratio QUE/2HP-β-CD 2:1) dissolved in DMSO at 25 °C.

In Table 4, it is shown that the chemical shifts of QUE are shifted downfield. This is indicative that QUE is inducing complexing with 2HP-β-CD in accordance with fluorescence experiments, see Section 3.3 below. In addition, this downfield shift designates that the interactions are of hydrophobic nature. These interactions affect the magnetic

Table 4
Values in ppm of QUE alone, mixing of QUE with 2HP-β-CD (stoichiometry ratio 1:2) and dissolution of complex of QUE with 2HP-β-CD (stoichiometry ratio 1:2) in DMSO-d6 and in D_2O at 25 °C and 40 °C.

	H6′	H2′	H3′	H8	H6a	H6b	OH (7)	OH (5)	OH (3)	OH (3′)
					DMSO-d6					
QUE alone (25 °C)	8.352	7.675	7.557	6.888	6.412	6.187	10.844	12.487	9.638	9.364
QUE alone (40 °C)	8.036	7.664	7.540	6.885	6.414	6.186	10.750	12.455	9.500	9.243
Mix of QUE & 2HP-β-CD (25 °C)	8.029	7.647	7.540	6.880	6.403	6.179	–	12.485	–	9.359
Mix of QUE & 2HP-β-CD (40 °C)	7.756	7.660	7.538	6.882	6.402	6.184	–	12.451	–	9.243
Complex of QUE & 2HP-β-CD (25 °C)	8.048	7.685	7.540	6.884	6.413	6.184	10.730	12.483	–	9.330
Δ(QUE-Mix) (25 °C)	−0.323	−0.028	−0.017	−0.008	−0.009	−0.008	–	−0.002	-	−0.005
Δ(QUE-Mix) (40 °C)	−0.28	−0.004	−0.002	−0.003	−0.012	−0.012	–	−0.004	–	0
Δ(QUE-Complex) (25 °C)	−0.304	0.01	−0.017	−0.004	0.001	−0.003	–	−0.004	–	−0.034
Δ(mix-complex) (25 °C)	0.019	0.038	0	0.004	0.01	0.005	–	−0.002	–	−0.029
					D_2O					
QUE alone (25 °C)	7.703	7.600	7.028	6.693	5.865	5.892				
QUE alone (40 °C)	7.601	7.600	7.020	6.678	5.777	5.789				
Mix of QUE & 2HP-β-CD (25 °C)	7.550	7.460	6.861	6.508	5.774	5.773				
Mix of QUE & 2HP-β-CD(40 °C)	7.756	7.750	7.671	7.052	6.751	6.432				
Complex (QUE &2HP-β-CD) (25 °C)	8.397	7.575	7.431	6.913	6.565	6.218				
Δ(QUE-Mix) (25 °C)	−0.153	−0.160	−0.167	−0.185	−0.09	−0.119				
Δ(QUE-Mix) (40 °C)	0.155	0.15	0.651	0.374	0.974	0.643				
Δ (QUE-Complex) (25 °C)	0.694	−0.025	0.403	0.220	0.700	0.326				
Δ(mix-complex) (25 °C)	0.847	0.115	0.57	0.405	0.7	0.326				

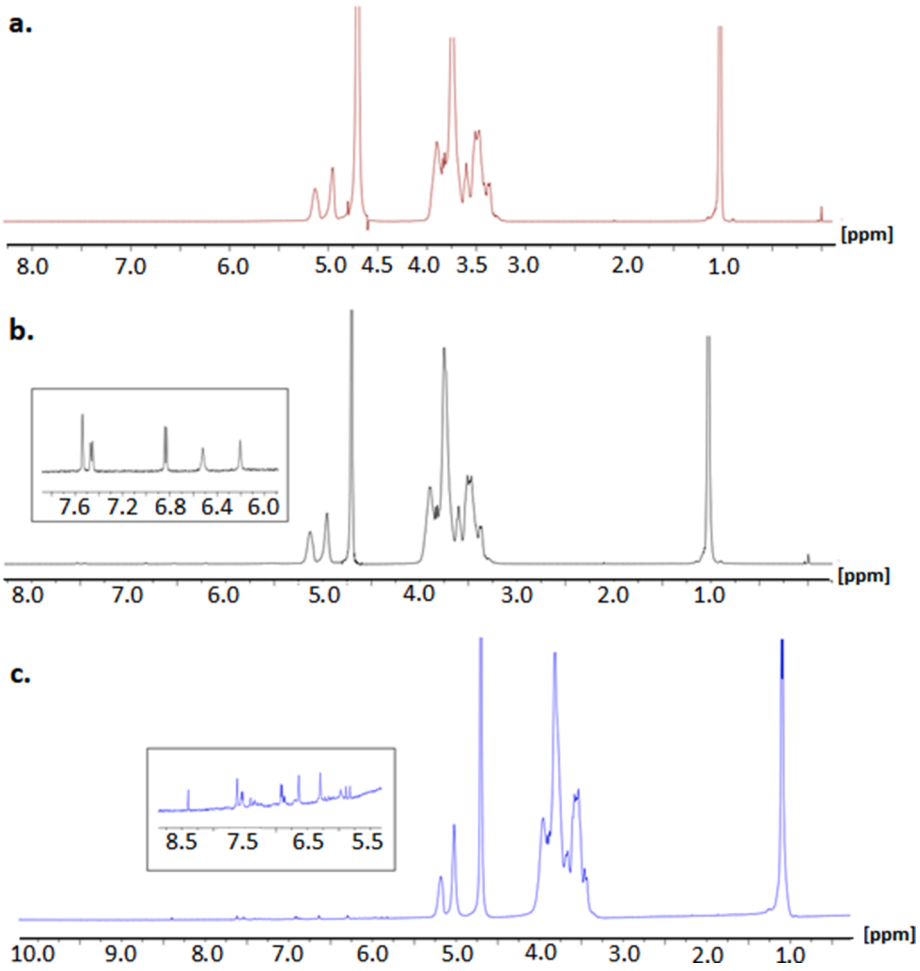

Fig. 6. Spectra of (a) 2HP-β-CD, (b) mixing of (a) and (b) with a stoichiometry ratio 1:2 and (c) dissolution of complex of QUE with 2HP-β-CD in D_2O (stoichiometry ratio 1:2) at 25 °C using a 400 MHz spectrometer.

anisotropy system of QUE created by the aromatic π-electrons. Same results are obtained also at 40 °C (not shown) depicting that its incorporation properties do not depend on the temperature. According to the literature [45] a chemical shift at 12.25 ppm is observed for QUE in CD_3OH solvent attributed to the intramolecular hydrogen bonding between C5 (OH) and C4 (C = O). It is also of interest to observe that this

Table 5
Values in ppm of 2HP-β-CD alone, mixing of QUE with 2HP-β-CD (stoichiometry ratio 1:2) and dissolution of complex of QUE with 2HP-β-CD in DMSO-d6 and in D_2O at 25 °C and 40 °C (stoichiometry ratio 1:2).

	H1	H1	H8*	H3*	H6*	H2*-H4*-H5*	H7*	H9*
				DMSO-*d6*				
2HP-β-CD alone (25 °C)	5.029	4.836	3.744	3.615	3.564	3.306	3.216	1.019
2HP-β-CD alone (40 °C)	5.021	4.839	3.774	3.629	3.575	3.336	3.287	1.032
Mix of QUE & 2HP-β-CD (25 °C)	5.012	4.833	3.750	3.612	3.554	3.304	3.228	1.020
Mix of QUE & 2HP-β-CD (40 °C)	5.030	4.848	3.771	3.643	3.581	3.315	3.298	1.037
Complex of QUE & 2HP-β-CD (25 °C)	5.022	4.843	3.758	3.630	3.560	3.312	3.332	1.020
Δ(2HP-β-CD- mix) (25 °C)	−0.017	−0.003	0.006	−0.003	−0.01	0.009	0.012	0.001
Δ(2HP-β-CD- mix) (40 °C)	0.009	0.009	−0.027	0.014	0.006	−0.021	0.011	0.005
Δ(2HP-β-CD - Complex (25 °C)	−0.007	0.007	0.014	0.015	−0.004	0.006	0.116	0.001
Δ(mix-complex) (25 °C)	0.01	0.01	0.008	0.018	0.076	0.008	0.104	0
				D_2O				
2HP-β-CD alone (25 °C)	5.031	4.921	3.873	3.752	3.587	3.476	3.372	1.019
2HP-β-CD alone (40 °C)	5.030	4.912	3.880	3.756	3.590	3.430	3.361	1.017
Mix of QUE & 2HP-β-CD (25 °C)	5.033	4.921	3.876	3.754	3.543	3.436	3.366	1.019
Mix of QUE & 2HP-β-CD (40 °C)	5.022	4.903	3.865	3.751	3.580	3.422	3.328	1.017
Complex of QUE & 2HP-β-CD (25 °C)	5.030	4.922	3.867	3.752	3.544	3.433	3.363	1.019
Δ(2HP-β-CD - mix) (25 °C)	0.002	0	0.003	0.002	−0.044	−0.04	0.006	0
Δ(2HP-β-CD - mix) (40 °C)	−0.008	−0.009	−0.015	−0.005	−0.010	−0.008	−0.033	0
Δ(2HP-β-CD - Complex (25 °C)	−0.001	0.001	−0.006	0.115	−0.043	−0.043	−0.009	0
Δ(mix-complex) (25 °C)	−0.003	0.001	−0.009	−0.002	0.001	−0.003	−0.003	0

hydrogen bonding between C5 (OH) and C4 (C = O) is conserved when QUE is engulfed in 2HP-β-CD in DMSO-d6 solvent designing that is independent of the environment. The chemical shifts at 10.7, 9.6 and 9.3 ppm attributed to OH(7), OH(3) and OH(3′) correspondingly of QUE show significant changes in the complexing form with 2HP-β-CD. Thus, the peak at 10.7 ppm disappears and the peaks at 9.6 ppm and 9.3 ppm match and form a significantly broad peak.

Fig. 6 shows ^{1}H NMR spectra results of 2HP-β-CD, mixture of 2HP-β-CD with QUE and their complex dissolved in D_2O. QUE was not dissolved in D_2O both at 25 °C and 40 °C. As a result, peaks of QUE are not eminent, and especially peaks of OH(7), OH(5),OH(3) and OH(3′) are not depicted. As it can be depicted from spectra, the peak both in the stoichiometric mixture and complex of QUE with 2HP-β-CD (1:2) are well resolved. This means that QUE solubility is increased considerably when it is in the complex form. Chemical shifts of 2HP-β-CD alone and in the complex form are shown in Table 4. Δδ values in Table 4, indicated a reduction in chemical shifts when QUE and 2HP-β-CD are in mixing sample in D_2O at 25 °C and an increase at 40 °C and in the mostly in the complex form. This is indicative that there are deshielding and shielding areas when QUE is mixing or complexing with 2HP-β-CD as with the solvent DMSO-d6.

In Table 5 are shown the chemical shifts changes of 2HP-β-CD in absence and presence of QUE in DMSO-d6 and D_2O at 25 °C and 40 °C. The chemical shifts of 2HP-β-CD did not modify significantly during complexing. Δδ values were both negative and positive after complexing relatively to 2HP-β-CD alone indicating the different upfield and downfield effects that QUE exerts on the different regions of 2HP-β-CD. It is of interest that at 40 °C in D_2O the differences were only downfield. However, these differences were very small generally.

Fig. 7 shows ^{1}H NMR spectra of QUE and 2,6Me-β-CD alone, their mixture using the stoichiometry ratio QUE:2,6Me-β-CD 2:1 in DMSO-d6 and their complex (stoichiometry ratio QUE:2,6Me-β-CD 1:2) dissolved in DMSO at 25 °C. In Table 6, it is observed that the chemical shifts of QUE are shifted downfield, when it is mixed at a stoichiometry ratio 1:2 with 2,6Me-β-CD in DMSO-d6 at 25 °C and 40 °C. Similar reduction is noted in case of complex of QUE with 2,6Me-β-CD. Similar changes were observed in QUE at the peaks OH(7), OH(3) and OH(3′) when was mixed or complexed with 2,6Me-β-CD to those of 2HP-β-CD. No significant change was observed in the intramolecular hydrogen bonding between C5 (OH) and C4 (C = O) as was observed also with 2HP-β-CD.

Fig. 8 shows ^{1}H NMR spectra results of 2,6Me-β-CD, mixture (stoichiometry ratio 2:1) of 2,6Me-β-CD with QUE and their complex (stoichiometry ratio 2:1) dissolved in D_2O. QUE was not dissolved in D_2O both at 25 °C and 40 °C as it is already mentioned above. As it can be depicted from spectra, the peaks both in the mixture and complex of QUE are well resolved. This means that QUE solubility is increased considerably when it is in the complex form. Chemical shifts of 2,6Me-β-CD alone and in the complex form are shown in Table 6. Protons of QUE mixing with 2,6Me-β-CD at a stoichiometry ratio in D_2O at 25 °C, were noticed to have shifted upfield and downfield, while at 40 °C and in the complex form have shifted only downfield. Finally, in Table 7 are shown the chemical shifts changes of 2,6Me-β-CD in absence and presence of QUE in DMSO-d6 and D_2O at 25 °C and 40 °C. Both downfield and upfield changes were observed as in the 2HP-β-CD. The chemical shifts of 2,6Me-β-CD did not modify significantly during complexing.

NMR spectra show that QUE is inducing complexing with 2HP-β-CD and 2,6Me-β-CD (1:2 stoichiometry ratio) in accordance with fluorescence experiments (Section 3.3) and DFT calculations (Section 3.1) resulting in an increased QUE solubility. Finally, the phase solubility studies in a mixture of QUE with 2HP-β-CD or 2,6Me-β-CD[20] show a positive deviation from the linearity, observed mainly in 2HP-β-CD at pH 6.8, which can be probably attributed to the further formation of a 1:2 (QUE/CD) complex. This deviation, observed mainly in 2HP-β-CD is in accordance with the present calculations, where the QUE is binding stronger in the 2HP-β-CD_2 dimeric assembly. It should be noted that the ONIOM(DFT:PM6) and DFT calculations have been performed on minimum-energy snapshots of the systems, and despite that these snapshots were not obtained over a simulation trajectory, they can be considered highly representative and accurate.

3.3. *Fluorescence spectroscopy*

The stoichiometry of the formed complexes was determined using Job's plot method by plotting the alternation of the fluorescent signal at 550 nm against the molar fraction of QUE (Fig. 9). The maximum alternation of the fluorescent signal in both cases was observed at a mole fraction of 0.35 indicating the formation of 1:2 complexation between QUE and the CDs, in excellent agreement with our DFT calculations that predict the existence the CD's dimeric assemblies and the encapsulation of QUE in them, in accordance with the present NMR spectra and the phase solubility studies [20].

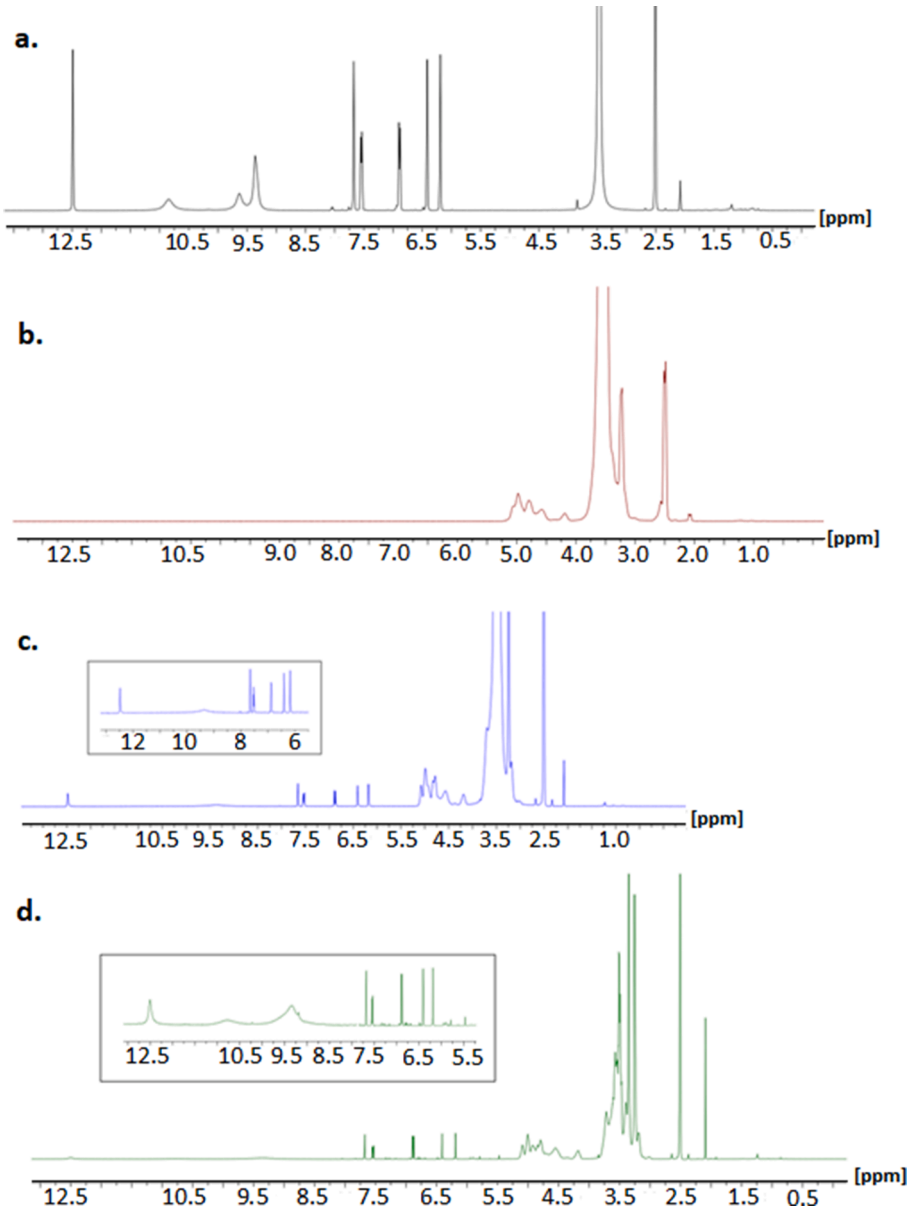

Fig. 7. Spectra of (a) QUE, (b) 2,6Me-β-CD, (c) mixing of (a) and (b) with stoichiometry ratio 1:2 and (d) dissolution of complex of QUE with 2,6Me-β-CD in DMSO-d6 at 25 °C (stoichiometry ratio 1:2) using a 400 MHz spectrometer.

4. Summary and conclusions

In the present work, we attempt to deepen our understanding on the binding modes of QUE with the aforementioned CDs by investigating the requisite QUE:CDs stoichiometry that gives rise to favorable complexation. Specifically, we study the entrapment of QUE in two capsules formed by 2HP-β-CD and 2,6Me-β-CD, employing NMR spectroscopy, fluorescent spectroscopy, and DFT calculations. In the CD cage, QUE is separated from solvent molecules by mechanical barriers, and it can consequently be carried in water solutions. In fact, the CD capsule functions as the solvent surrounding the solute.

Here, it was revealed via theoretical and experimental methodologies, i.e., DFT calculations, NMR spectroscopy and Fluorescence Spectroscopy, that the QUE:CDs stoichiometry for optimal complex formation follows a 1:2 pattern, where one QUE molecule is associated with two different CD molecules (namely, 2HP-β-CD and 2,6Me-β-CD.

DFT calculations have shown that both dimeric assemblies and the encapsulated complexes of QUE with them are stable. However, the 2HP-β-CD_2 dimeric assembly is more stable than 2,6Me-β-CD_2, while the QUE molecule in 2HP-β-CD_2 is better encapsulated than in 2,6Me-β-CD_2. NMR spectroscopy has shown that the NMR ^{1}H chemical shifts of QUE are shifted downfield, indicating that QUE is complexed via hydrophobic interactions with the two CDs. QUE solubility is increased considerably when it is encapsulated in the dimeric assemblies. It is interesting that similar results are obtained at 25 °C and 40 °C depicting that its incorporation properties do not depend on the temperature. Finally, fluorescence spectroscopy shows that the stoichiometry of the formed complexes, determined via the Job's plot method,is 1:2.

Finally, the positive deviation from the linearity phase solubility studies found in mixtures of QUE with 2HP-β-CD or 2,6Me-β-CD which was observed mainly in 2HP-β-CD at pH 6.8 and it was attributed to the further formation of a 1:2 (QUE:CD) complex, [20] is in accordance with the present calculations, where the QUE binds stronger in the 2HP-β-CD_2 dimeric assembly. It should be noted that DFT calculations have been performed on minimum-energy snapshots of the systems, and even though these snapshots were not obtained over a simulation trajectory, they can be considered highly representative and accurate.

Furthermore, it is found that the encapsulation influences the

Table 6
Values in ppm of QUE alone, mixing of QUE with 2,6Me-β-CD (stoichiometry ratio 1:2) and dissolution of complex of QUE with 2,6Me-β-CD in DMSO-d6 and in D_2O at 25 °C and 40 °C (stoichiometry ratio 1:2).

	H6′	H2′	H3′	H8	H6a	H6b	OH (7)	OH (5)	OH (3)	OH (3′)
					DMSO					
QUE alone (25 °C)	8.352	7.675	7.557	6.888	6.412	6.187	10.844	12.487	9.638	9.364
QUE alone (40 °C)	8.036	7.664	7.540	6.885	6.414	6.186	10.750	12.455	9.500	9.243
Mix of QUE & 2,6Me-β-CD (25 °C)	8.038	7.656	7.531	6.876	6.401	6.181	–	12.480	–	9.348
Mix of QUE & 2,6Me-β-CD (40 °C)	8.020	7.632	7.520	6.880	6.388	6.150	–	12.415	–	9.244
Complex of QUE & 2,6Me-β-CD (25 °C)	8.033	7.668	7.533	6.879	6.396	6.182	10.775	12.500		9.334
Δ(QUE-Mix) (25 °C)	−0.332	−0.019	−0.026	−0.012	−0.011	−0.006		−0.007		−0.016
Δ(QUE-Mix) (40 °C)	−0.016	−0.032	−0.02	−0.005	−0.026	−0.036		−0.04		0.001
Δ(QUE-Complex(25 °C)	−0.319	−0.007	−0.024	−0.009	−0.016	−0.005	−0.069	0.013		−0.03
Δ(mix-Complex) (25 °C)	−0.005	0.012	0.013	0.003	−0.005	−0.001		0.02		0.014
					D_2O					
QUE alone (25 °C)	7.703	7.600	7.028	6.693	5.865	5.892				
QUE alone (40 °C)	7.601	7.600	7.020	6.678	5.777	5.789				
Mix of QUE & 2,6Me-β-CD (25 °C)	7.55	7.473	6.924	6.478	5.910	5.940				
Mix of QUE & 2,6Me-β-CD (40 °C)	7.698	7.632	7.520	6.880	6.388	6.150				
Complex of QUE & 2,6Me-β-CD (25 °C)	8.403	7.608	7.544	6.921	6.634	6.291				
Δ(QUE-Mix) (25 °C)	−0.153	−0.127	−0.104	−0.215	0.045	0.048				
Δ(QUE-Mix) (40 °C)	0.097	0.032	0.500	0.202	0.611	0.361				
Δ(QUE-Complex(25 °C)	0.700	0.008	0.516	0.228	0.769	0.399				
Δ(mix-Complex) (25 °C)	0.853	0.135	0.62	0.443	0.724	0.351				

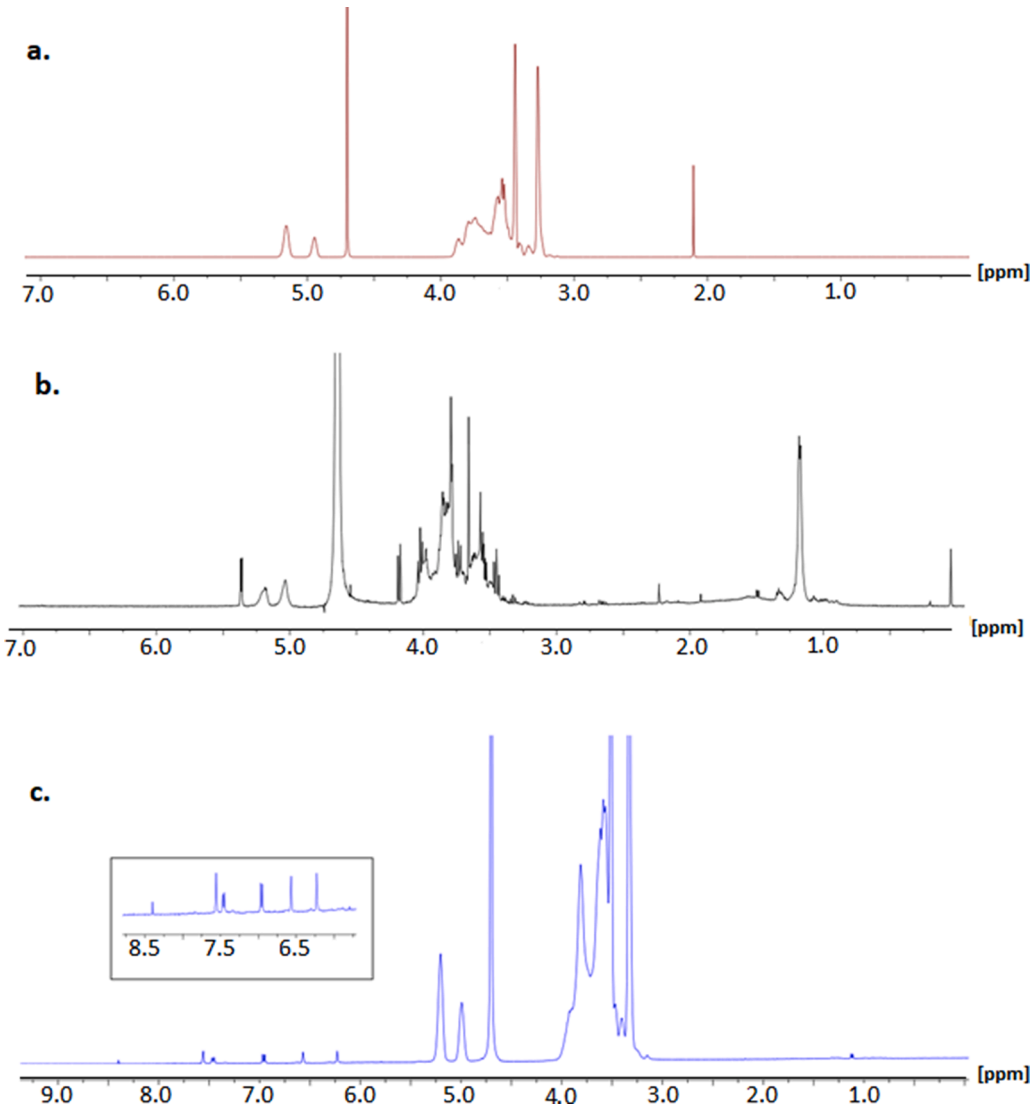

Fig. 8. Spectra of (a) QUE, (b) 2,6Me-β-CD, (c) mixing of (a) and (b) (stoichiometry ratio 1:2) and (d) dissolution of complex of QUE with 2,6Me-β-CD in D_2O at 25 °C (stoichiometry ratio 1:2) using a 400 MHz spectrometer.

Table 7
Values in ppm 2,6Me-β-CD alone, mixing of QUE with 2,6Me-β-CD (stoichiometry ratio 1:2) and dissolution of complex of QUE with 2,6Me-β-CD (1:2 stoichiometry ratio) in DMSO-d6 and in D_2O at 25 °C and 40 °C.

	H1a′′	H1b′′	H3′′	H5′′	H6′′	H2′′	H4′′	H6-O-Me	H2′′	H2-O-Me
				DMSO						
2,6Me-β-CD alone (25 °C)	5.069	4.980	3.703	3.554	3.533	3.520	3.520	3.503	3.387	3.241
2,6Me-β-CD alone (40 °C)	5.055	4.980	3.668	3.543	3.513	3.503	3.503	3.480	3.380	3.220
Mixture of QUE &2,6Me-β-CD (25 °C)	5.032	4.878	3.656	3.500	3.512	3.497	3.486	3.500	3.332	3.240
Mixture of QUE &2,6Me-β-CD(40 °C)	5.023	4.866	3.632	3.500	3.514	3.490	3.459	3.502	3.323	3.221
Complex of QUE &2,6Me-β-CD (25 °C)	5.091	5.000	3.712	3.560	3.501	3.916	3.912	3.920	3.342	3.250
Δ(2,6Me-β-CD- mix) (25 °C)	−0.037	−0.102	−0.047	−0.054	−0.021	−0.023	−0.017	−0.003	−0.055	−0.001
Δ(2,6Me-β-CD - mix) (40 °C)	−0.023	−0.114	−0.036	−0.043	0.001	−0.013	−0.044	0.022	0.057	0.001
Δ(2,6Me-β-CD - Complex) (25 °C)	0.022	0.02	0.009	0.006	−0.032	0.396	0.392	0.417	−0.045	0.009
Δ (mix-Complex) (25 °C)	0.059	0.122	0.056	0.06	−0.011	0.449	0.426	0.420	0.01	0.010
				D_2O						
2,6Me-β-CD alone (25 °C)	5.391	5.091	4.012	3.940	3.914	3.702	3.686	3.591	3.497	3.413
2,6Me-β-CD alone (40 °C)	5.387	5.081	4.004	3.922	3.918	3.689	3.675	3.567	3.457	3.321
Mixture of QUE &2,6Me-β-CD (25 °C)	5.291	5.034	4.003	3.907	3.888	3.683	3.677	3.593	3.442	3.420
Mixture of QUE &2,6Me-β-CD (40 °C)	5.219	5.059	4.182	4.003	3.866	3.643	3.632	3.509	3.408	3.399
Complex of QUE &2,6Me-β-CD (25 °C)	5.290	5.031	4.001	3.900	3.888	3.679	3.667	3.589	3.439	3.417
Δ(2,6Me-β-CD-mix (25 °C)	−0.100	−0.057	−0.009	−0.033	−0.026	−0.019	−0.009	0.002	−0.055	0.007
Δ(2,6Me-β-CD /mix) (40 °C)	−0.168	−0.022	0.178	0.081	−0.052	−0.046	−0.043	−0.049	−0.049	0.078
Δ(2,6Me-β-CD/ Complex (25 °C)	−0.101	−0.06	−0.011	−0.04	−0.026	−0.023	−0.019	−0.002	−0.058	0.004
Δ(mix-complex) (25 °C)	−0.001	−0.003	−0.002	−0.007	0	−0.01	−0.01	0.084	−0.003	−0.003

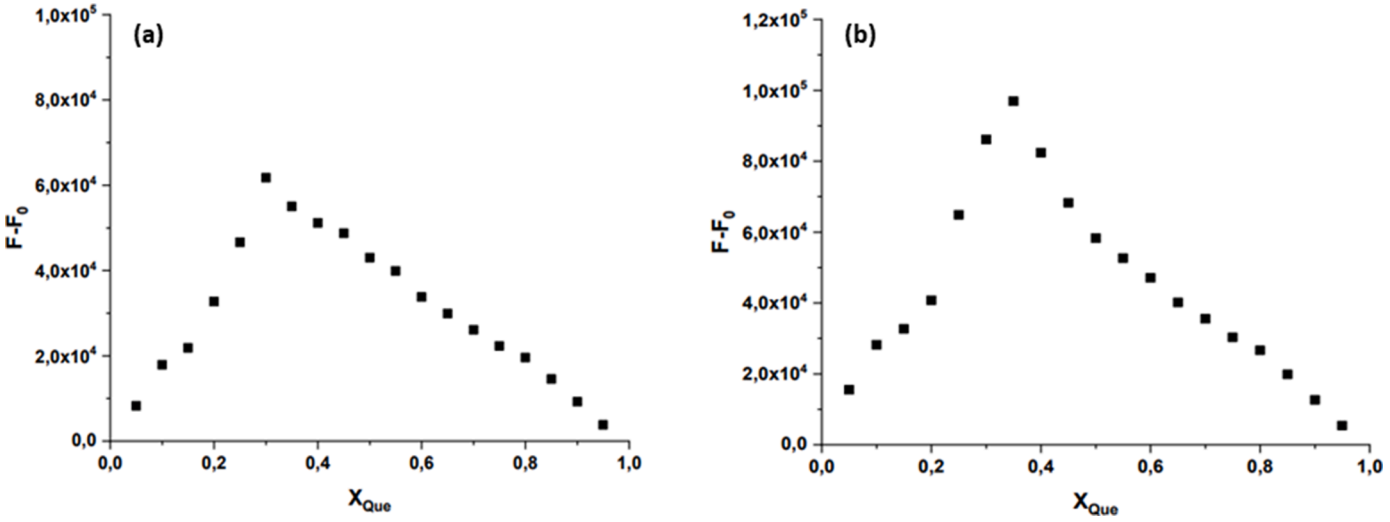

Fig. 9. Job plot for the determination of the binding stoichiometry of QUE and CDs; (a)2HP-β-CD and (b) 2,6Me-β-CD.

absorption spectra of QUE, i.e., red and blue shifts are observed as well as differences in the intensity of the peaks. Finally, the cage affects the electron density of the QUE. It is of interest that the major peaks of the QUE, in the dimeric assemblies, at about 250 nm and 200 nm, correspond to partially charge transfer (CT) excitations or to a full CT. This fact is not common, and it has not been observed in the QUE in solution. Finally, for the encapsulated QUE in CDs, the calculated $T_1 \rightarrow S_0$ vertical de-excitation is about 570 nm in the single CDs and about 800 nm in the dimeric complexes, showing that these complexes have the potential to be used as candidates for PDT.

Credit author statement

Georgios Leonis: Introduction: investigation, writing-original draft

Vasiliki Vakali: NMR spectroscopy: investigation, data curation, formal analysis, writing-original draft

Nikoletta Zoupanou: NMR spectroscopy: investigation, data curation, formal analysis, visualization. writing original draft

Nikitas Georgiou: DFT calculations: investigation, data curation, formal analysis, visualization, writing original draft.

Dimitrios A. Diamantis: Fluorescent spectroscopy: investigation, data curation, formal analysis, writing original draft

Andreas G. Tzakos: Fluorescent spectroscopy: methodology, investigation, resourses, supervision, writing original draft

Thomas Mauromoustakos: NMR sppectroscopy: methodology, investigation, resourses, supervision, writing original draft.

Demeter Tzeli: Conceptualization, data curation, investigation, formal analysis methodology, project administration, resources, supervision, visualization, writing–original draft, writing-review & editing

Supporting information

Figs. S1–S3: Calculated minimum structures of QUE@2HP-β-CD, QUE@2,6Me-β-CD, QUE@2HP-β-CD2 and QUE@2,6Me-β-CD2. Fig. S4. Frontier Molecular Orbitals. Figs. S5–S12. MMR Spectra.

Declaration of Competing Interest

The authors declare that they have no known competing financial interests or personal relationships that could have appeared to influence

the work reported in this paper.

Data availability

Data will be made available on request.

Supplementary materials

Supplementary material associated with this article can be found, in the online version, at doi:10.1016/j.molstruc.2023.136430.

References

[1] World Health Organization. https://www.who.int/health-topics/cancer#tab=tab_1.
[2] S. Chakraborty, T. Rahman, The difficulties in cancer treatment, Ecancermedicalscience 6 (2012) ed16.
[3] L. Zhong, Y. Li, L. Xiong, W. Wang, M. Wu, T. Yuan, W. Yang, C. Tian, Z. Miao, T. Wang, S. Yang, Small molecules in targeted cancer therapy: advances, challenges, and future perspectives, Sign. Transduct. Target. Ther. 6 (1) (2021) 201.
[4] M.C. Dias, D. Pinto, A.M.S. Silva, Plant flavonoids: chemical characteristics and biological activity, Molecules 26 (17) (2021).
[5] L.G.S. Ponte, I.C.B. Pavan, M.C.S. Mancini, L.G.S. da Silva, A.P. Morelli, M. B. Severino, R.M.N. Bezerra, F.M. Simabuco, The hallmarks of flavonoids in cancer, Molecules 26 (7) (2021).
[6] D. Procházková, I. Boušová, N. Wilhelmová, Antioxidant and prooxidant properties of flavonoids, Fitoterapia 82 (4) (2011) 513–523.
[7] R. Wang, L. Yang, S. Li, D. Ye, L. Yang, Q. Liu, Z. Zhao, Q. Cai, J. Tan, X. Li, Quercetin inhibits breast cancer stem cells via downregulation of aldehyde dehydrogenase 1A1 (ALDH1A1), chemokine receptor type 4 (CXCR4), mucin 1 (MUC1), and epithelial cell adhesion molecule (EpCAM), Med. Sci. Monit. 24 (2018) 412–420.
[8] A.B. Granado-Serrano, M.A. Martín, L. Bravo, L. Goya, S. Ramos, Quercetin induces apoptosis via caspase activation, regulation of Bcl-2, and inhibition of PI-3-kinase/Akt and ERK pathways in a human hepatoma cell line (HepG2), J. Nutr. 136 (11) (2006) 2715–2721.
[9] P. Asgharian, A.P. Tazekand, K. Hosseini, H. Forouhandeh, T. Ghasemnejad, M. Ranjbar, M. Hasan, M. Kumar, S.M. Beirami, V. Tarhriz, S.R. Soofiyani, L. Kozhamzharova, J. Sharifi-Rad, D. Calina, W.C. Cho, Potential mechanisms of quercetin in cancer prevention: focus on cellular and molecular targets, Cancer Cell Int. 22 (1) (2022) 257.
[10] H. Zalpoor, M. Nabi-Afjadi, R. Forghaniesfidvajani, C. Tavakol, F. Farahighasreaboonasr, F. Pakizeh, V.G. Dana, F. Seif, Quercetin as a JAK-STAT inhibitor: a potential role in solid tumors and neurodegenerative diseases, Cell. Mol. Biol. Lett. 27 (1) (2022) 60.
[11] G. D'Andrea, Quercetin: a flavonol with multifaceted therapeutic applications? Fitoterapia 106 (2015) 256–271.
[12] W. Wang, C. Sun, L. Mao, P. Ma, F. Liu, J. Yang, Y. Gao, The biological activities, chemical stability, metabolism and delivery systems of quercetin: a review, Trend. Food Sci. Technol. 56 (2016) 21–38.
[13] G. Crini, Review: a history of cyclodextrins, Chem. Rev. 114 (21) (2014) 10940–10975.
[14] A. Singh, A. Kaler, V. Singh, R. Patil, U.C. Banerjee, Cyclodextrins and biotechnological applications, cyclodextrins in pharmaceutics, Cosmetics Biomed. (2011) 275–285.
[15] S.B. Carneiro, F. Costa Duarte, L. Heimfarth, J.S. Siqueira Quintans, L.J. Quintans-Júnior, V.F.D. Veiga Júnior, A.N. de Lima Á, Cyclodextrin¯drug inclusion complexes: in vivo and in vitro approaches, Int. J. Mol. Sci. 20 (3) (2019).
[16] N. Wangsawangrung, C. Choipang, S. Chaiarwut, P. Ekabutr, O. Suwantong, P. Chuysinuan, S. Techasakul, P. Supaphol, Quercetin/hydroxypropyl-β-cyclodextrin inclusion complex-loaded hydrogels for accelerated wound healing, Gels 8 (9) (2022) 573.
[17] T.F. Kellici, M.V. Chatziathanasiadou, D. Diamantis, A.V. Chatzikonstantinou, I. Andreadelis, E. Christodoulou, G. Valsami, T. Mavromoustakos, A.G. Tzakos, Mapping the interactions and bioactivity of quercetin-(2-hydroxypropyl)-beta-cyclodextrin complex, Int. J. Pharm. 511 (1) (2016) 303–311.
[18] R. Rajamohan, M. Murugan, A. Anitha, Y.R. Lee, F. Madi, N. Leila, M. Viswalingam, Interaction of chloroquine with 2-(hydroxypropyl)-β-cyclodextrin through the supramolecular assembly for cytotoxicity on breast cancer cell lines, Monatshefte für Chemie - Chemical Monthly 153 (12) (2022) 1171–1184.
[19] M. Murugan, R. Rajamohan, A. Anitha, M. Fatiha, Non-covalent bonding interaction between primaquine as guest and 2-(hydroxypropyl)-β-cyclodextrin as host, Polycycl. Aromat. Compd. 42 (4) (2022) 1861–1878.
[20] K. Manta, P. Papakyriakopoulou, M. Chountoulesi, D.A. Diamantis, D. Spaneas, V. Vakali, N. Naziris, M.V. Chatziathanasiadou, I. Andreadelis, K. Moschovou, I. Athanasiadou, P. Dallas, D.M. Rekkas, C. Demetzos, G. Colombo, S. Banella, U. Javornik, J. Plavec, T. Mavromoustakos, A.G. Tzakos, G. Valsami, Preparation and biophysical characterization of quercetin inclusion complexes with β-cyclodextrin derivatives to be formulated as possible nose-to-brain quercetin delivery systems, Mol. Pharm. 17 (11) (2020) 4241–4255.
[21] S.-L. Yang, L.-J. Zhao, S.-M. Chi, J.-J. Du, Q. Ruan, P.-L. Xiao, Y. Zhao, Inclusion complexes of flavonoids with propylenediamine modified β-cyclodextrin: preparation, characterization and antioxidant, J. Mol. Struct. 1183 (2019) 118–125.
[22] V. Palli, G. Leonis, N. Zoupanou, N. Georgiou, M. Chountoulesi, N. Naziris, D. Tzeli, C. Demetzos, G. Valsami, K.D. Marousis, G.A. Spyroulias, T. Mavromoustakos, Losartan Interactions with 2-Hydroxypropyl-β-CD, Molecules 27 (8) (2022).
[23] A. Praveena, S. Prabu, F. Madi, R. Rajamohan, Theoretical investigation of inclusion complexes of 3-hydroxyflavone and quercetin as guests with native and modified β-cyclodextrins as hosts, Polycycl. Aromat. Compd. 43 (1) (2023) 141–153.
[24] Q. Guo, C. Jiang, Delivery strategies for macromolecular drugs in cancer therapy, Acta Pharm. Sin. B 10 (6) (2020) 979–986.
[25] V. Vakali, M. Papadourakis, N. Georgiou, N. Zoupanou, D.A. Diamantis, U. Javornik, P. Papakyriakopoulou, J. Plavec, G. Valsami, A.G. Tzakos, D. Tzeli, Z. Cournia, T. Mauromoustakos, Comparative interaction studies of quercetin with 2-hydroxyl-propyl-β-cyclodextrin and 2,6-methylated-β-cyclodextrin, Molecules 27 (17) (2022) 5490.
[26] Z. Bikadi, E. Hazai, Application of the PM6 semi-empirical method to modeling proteins enhances docking accuracy of AutoDock, J. Cheminform. 1 (1) (2009) 15.
[27] T. Vreven, K. Morokuma, Chapter 3 hybrid methods: ONIOM(QM:MM) and QM/MM, Annu. Rep. Comput. Chem. 2 (2006) 35–51.
[28] A.D. Becke, A new mixing of Hartree–Fock and local density-functional theories, J. Chem. Phys. 98 (2) (1993) 1372–1377.
[29] L.A. Curtiss, M.P. McGrath, J.P. Blaudeau, N.E. Davis, R.C. Binning Jr, L. Radom, Extension of Gaussian-2 theory to molecules containing third-row atoms Ga–Kr, J. Chem. Phys. 103 (14) (1995) 6104–6113.
[30] D. Tzeli, G. Theodorakopoulos, I.D. Petsalakis, D. Ajami, J. Rebek Jr, Conformations and fluorescence of encapsulated stilbene, J. Am. Chem. Soc. 134 (9) (2012) 4346–4354.
[31] T. Vreven, K. Morokuma, O. Farkas, H.B. Schlegel, M.J. Frisch, Geometry optimization with QM/MM, ONIOM, and other combined methods. I. Microiterations and constraints, J. Comput. Chem. 24 (6) (2003) 760–769.
[32] C.E. Tzeliou, M.A. Mermigki, D. Tzeli, Review on the QM/MM methodologies and their application to metalloproteins, Molecules 27 (9) (2022).
[33] D. Tzeli, P.G. Tsoungas, I.D. Petsalakis, P. Kozielewicz, M. Zloh, Intramolecular cyclization of β-nitroso-o-quinone methides. A theoretical endoscopy of a potentially useful innate 'reclusive' reaction, Tetrahedron 71 (2) (2015) 359–369.
[34] M. Cossi, G. Scalmani, N. Rega, V. Barone, New developments in the polarizable continuum model for quantum mechanical and classical calculations on molecules in solution, J. Chem. Phys. 117 (1) (2002) 43–54.
[35] K.W. Street, W.E. Acree, Estimation of the effective dielectric constant of cyclodextrin cavities based on the fluorescence properties of pyrene-3-carboxaldehyde, Appl. Spectrosc. 42 (7) (1988) 1315–1318.
[36] D. Saric, M. Kohns, J. Vrabec, Dielectric constant and density of aqueous alkali halide solutions by molecular dynamics: a force field assessment, J. Chem. Phys. 152 (16) (2020), 164502.
[37] M.J. Frisch, G.W. Trucks, H.B. Schlegel, G.E. Scuseria, M.A. Robb, J.R. Cheeseman, G. Scalmani, V. Barone, G.A. Petersson, H. Nakatsuji, X. Li, M. Caricato, A. V. Marenich, J. Bloino, B.G. Janesko, R. Gomperts, B. Mennucci, H.P. Hratchian, J. V. Ortiz, A.F. Izmaylov, J.L. Sonnenberg, Williams, F. Ding, F. Lipparini, F. Egidi, J. Goings, B. Peng, A. Petrone, T. Henderson, D. Ranasinghe, V.G. Zakrzewski, J. Gao, N. Rega, G. Zheng, W. Liang, M. Hada, M. Ehara, K. Toyota, R. Fukuda, J. Hasegawa, M. Ishida, T. Nakajima, Y. Honda, O. Kitao, H. Nakai, T. Vreven, K. Throssell, J.A. Montgomery Jr, J.E. Peralta, F. Ogliaro, M.J. Bearpark, J.J. Heyd, E.N. Brothers, K.N. Kudin, V.N. Staroverov, T.A. Keith, R. Kobayashi, J. Normand, K. Raghavachari, A.P. Rendell, J.C. Burant, S.S. Iyengar, J. Tomasi, M. Cossi, J. M. Millam, M. Klene, C. Adamo, R. Cammi, J.W. Ochterski, R.L. Martin, K. Morokuma, O. Farkas, J.B. Foresman, D.J. Fox, Gaussian 16 Rev. C.01, Wallingford, CT, 2016.
[38] D. Ntountaniotis, I. Andreadelis, T.F. Kellici, V. Karageorgos, G. Leonis, E. Christodoulou, S. Kiriakidi, J. Becker-Baldus, E.K. Stylos, M. V. Chatziathanasiadou, C.M. Chatzigiannis, D.E. Damalas, B. Aksoydan, U. Javornik, G. Valsami, C. Glaubitz, S. Durdagi, N.S. Thomaidis, A. Kolocouris, J. Plavec, A.G. Tzakos, G. Liapakis, T. Mavromoustakos, Host-guest interactions between candesartan and its prodrug candesartan cilexetil in complex with 2-hydroxypropyl-beta-cyclodextrin: on the biological potency for angiotensin II antagonism, Mol. Pharm. 16 (3) (2019) 1255–1271.
[39] L. Szente, J. Szejtli, Highly soluble cyclodextrin derivatives: chemistry, properties, and trends in development, Adv. Drug Deliv. Rev. 36 (1) (1999) 17–28.
[40] K. Robards, P.D. Prenzler, G. Tucker, P. Swatsitang, W. Glover, Phenolic compounds and their role in oxidative processes in fruits, Food Chem. 66 (4) (1999) 401–436.
[41] M. Buchweitz, P.A. Kroon, G.T. Rich, P.J. Wilde, Quercetin solubilisation in bile salts: a comparison with sodium dodecyl sulphate, Food Chem. 211 (2016) 356–364.
[42] J.P. Cornard, L. Dangleterre, C. Lapouge, Computational and spectroscopic characterization of the molecular and electronic structure of the Pb(II)-quercetin complex, J. Phys. Chem. A 109 (44) (2005) 10044–10051.
[43] X. Xiao, X. Zhao, X. Chen, J. Zhao, Heavy atom-free triplet photosensitizers: molecular structure design, photophysical properties and application in photodynamic therapy, Molecules 28 (5) (2023) 2170.
[44] H. Abrahamse, M.R. Hamblin, New photosensitizers for photodynamic therapy, Biochem. J. 473 (2016) 347–364.
[45] P. Charisiadis, V.G. Kontogianni, C.G. Tsiafoulis, A.G. Tzakos, M. Siskos, I. P. Gerothanassis, 1H-NMR as a structural and analytical tool of intra- and

intermolecular hydrogen bonds of phenol-containing natural products and model compounds, Molecules 19 (9) (2014) 13643–13682.